J COMP SCI APPL MATH

Journal of Computer Science and Applied Mathematics 1 (2014), 1–9
ISSN: 1857-9574 , UDC: 621.383.51:517.93 https://doi.org/10.37418/jcsam.1.1.1

SEMI-EMPIRICAL RELATION FOR AIR SPACE OF A SOLAR COLLECTOR

REHENA NASRIN[1], KHANDKER FARID UDDIN AHMED AND MD. ABDUL ALIM

ABSTRACT. The numerical problem of steady, laminar and incompressible natural convection flow in a wavy solar collector is studied. In this investigation, two vertical walls are perfectly insulated. The top cover glass surface is continuously absorbing solar energy. The bottom wavy solid surface is uniformly kept at a constant temperature T_c. Numerical analysis is done by this article for the performance of natural convective parameter (Ra) on flow and heat transfer phenomena inside a solar collector. The solar collector has the flat-plate cover and sinusoidal wavy absorber. Air (Prandtl number 0.7) is considered as the working fluid inside the solar collector. The governing partial differential equations with proper boundary conditions are solved by Finite Element Method using Galerkin's weighted residual scheme. The effect of Rayleigh number related to performance such as temperature and velocity distributions, convective heat transfer, mean temperature and velocity of air is investigated systematically. The results show that better performance of heat transfer inside the collector is found by using the highest value of Ra. Calculated average Nusselt number (Nu) is correlated with Rayleigh number (Ra) and Prandtl number (Pr). Then a semi-empirical relation is established from this correlation with experimental data.

1. INTRODUCTION

Solar energy, radiant light and heat from the sun, has been harnessed by humans since ancient times using a range of ever-evolving technologies. Of all the sources of renewable energy especially solar energy has the greatest potential when other sources in the country have depleted. Because of the desirable environmental and safety aspects it is widely believed that solar energy should be utilized instead of other alternative energy forms, even when the costs involved are slightly higher. Solar energy technologies include solar heating, solar photo voltaic, solar thermal electricity and solar architecture, which can make considerable contributions to solving some of the most urgent problems the world now faces.

Solar technologies are broadly characterized as either passive solar or active solar depending on the way they capture, convert and distribute solar energy. Active solar techniques include the use of photovoltaic panels and solar thermal collectors to harness the energy. Passive solar techniques include orienting a building to the Sun, selecting materials with favorable thermal mass or light dispersing properties, and designing spaces that naturally circulate air. The development of affordable, inexhaustible and clean solar energy technologies will have huge longer-term benefits. It will increase countries' energy security through reliance on an indigenous, inexhaustible and mostly import-independent resource, enhance substantiality, reduce pollution, lower the costs of mitigating climate change, and keep fossil fuel prices lower than otherwise. These advantages are global. Hence the additional costs of the incentives for early deployment should be considered learning investments; they must be wisely spent and need to be widely shared.

The analysis has been substantially assisted by the derivation of plate-fin efficiency factors. The factors relate the design and operating conditions of the collector in a systematic manner that facilitates prediction of heat collection rates at the design stage. The one-dimensional analysis offers a desired accuracy required in a routine analysis even though a two-dimensional temperature distribution exists over the absorber plate of the collector. Therefore, for more accurate analysis at low mass flow rates, a two-dimensional temperature distribution must be considered. Various investigators have used two dimensional conduction equations in their analysis with different boundary conditions.

[1] *corresponding author*

Key words and phrases. Free convection, solar collector, finite element method, Rayleigh number, correlation and semi-empirical relation.

Conventional analysis and design of solar collector is based on a one-dimensional conduction equation formulation of Sukhatme [1]. Stasiek [2] made experimental studies of heat transfer and fluid flow across corrugated and undulated heat exchanger surfaces. He concluded that the measuring technique comprising the use of LC flexible sheets and true-color processing might be used for a great variety of applications and should be of considerable use in improving the design of all types of compact heat exchanger. Noorshahi et al. [3] studied numerically the natural convection effect in a corrugated enclosure with mixed boundary conditions. Detailed experimental and numerical studies on the performance of the solar air heater were made by Gao [4] where the transport equations are discretized on a non-uniform mesh with a finite volume, fully implicit scheme, and the discretized equations are then solved with the S.O.R (successive over relaxation) iterative method.

There are so many methods introduced to increase the efficiency of the solar water heater by Xiaowu and Hua [5], Xuesheng et al. [6], Ho and Chen [7] and Hussain [8]. An innovative idea is to suspend ultra fine solid particles in the fluid for improving the thermal conductivity of the fluid by Hetsroni and Rozenblit [9]. The absorptance of the collector surface for shortwave solar radiation depends on the nature and colour of the coating and on the incident angle. Usually black colour is used. Various colour coatings had been proposed in Tripanagnostopoulos et al. [10], Orel et al. [11] and Wazwaz et al. [12] mainly for aesthetic reasons.

A low-cost mechanically manufactured selective solar absorber surface method had been proposed by Konttinen et al. [13]. Another category of collectors is the uncovered or unglazed solar collector by Soltau [14]. These are usually low-cost units which can offer cost effective solar thermal energy in applications such as water preheating for domestic or industrial use, heating of swimming pools of Molineaux et al. [15], space heating and air heating for industrial or agricultural applications. The principal requirement of the solar collector is a large contact area between the absorbing surface and the air. Various applications of solar air collectors were reported by Kolb et al. [16].

Kent [17] studied laminar natural convection in isosceles triangular enclosures for cold base and hot inclined walls numerically. Effects of Rayleigh number and aspect ratio on the flow field and heat transfer were analyzed. Results showed that the enclosures with a low aspect ratio had higher heat transfer rates from the bottom surface of the triangular enclosure. A numerical experiment is performed for inclined solar collectors by Varol and Oztop [18]. Results indicated that heat transfer was increased with increasing Rayleigh number and aspect ratio, and was decreased with increasing wavelength. Bég et al. [19] performed non-similar mixed convection heat and species transfer along an inclined solar energy collector surface with cross diffusion effects, where the resulting governing equations were transformed and then solved numerically using the local non similarity method and Runge-Kutta shooting quadrature.

Nasrin [20] investigated influences of physical parameters on mixed convection in a horizontal lid driven cavity with undulating base surface. Results showed that the wavy lid-driven cavity can be considered an effective heat transfer mechanism at larger wavy surface amplitude, as well as the number of waves and cavity aspect ratio.

From the above literature review it is mentioned that few numerical or experimental work has been done across air layer of solar collector. In spite of that there is a large scope to work with air flow and heat transfer by analyzing natural convection. In this article the natural convective flow and heat transfer are presented through a solar collector having sinusoidal-wave absorber. In addition a correlation among Nu, Ra and Pr is developed. Then a semi empirical relation is established with experimental data of Hollands et al. [21].

2. PHYSICAL MODELING

A schematic diagram of cross section of a solar collector is shown in Fig. 1. The fluid is assumed incompressible and the flow is considered to be laminar. If the cold water enters under the path of the wavy absorber then it becomes hot with contact of the absorber. Then this hot water can be used for household's usage or various purposes. The solar collector is a metal box with a glass cover plate on the top surface and a dark colored undulating absorber plate on the bottom. The bottom wavy wall is uniformly maintained at a constant temperature T_c. The top transparent surface is continuously absorbing solar energy. The density of the fluid is approximated by the Boussinesq model.

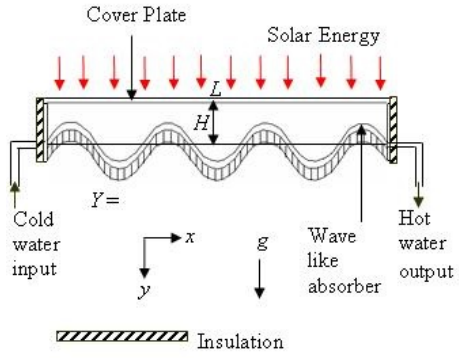

Fig. 1: Schematic diagram of the solar collector

3. MATHEMATICAL MODELING

The governing equations for steady laminar natural convection inside air space of a solar collector in terms of the Navier-Stokes and energy equation (dimensional form) are given as:

Continuity equation:

$$\frac{\partial u}{\partial x}+\frac{\partial v}{\partial y}=0\,.$$

x-momentum equation:

$$\rho(u\frac{\partial u}{\partial x}+v\frac{\partial u}{\partial y})=-\frac{\partial p}{\partial x}+\mu(\frac{\partial^2 u}{\partial x^2}+\frac{\partial^2 u}{\partial y^2})\,.$$

y-momentum equation:

$$\rho(u\frac{\partial v}{\partial x}+v\frac{\partial v}{\partial y})=-\frac{\partial p}{\partial y}+\mu(\frac{\partial^2 v}{\partial x^2}+\frac{\partial^2 v}{\partial y^2})+g\rho\beta(T-T_c)\,.$$

Energy equation:

$$u\frac{\partial T}{\partial x}+v\frac{\partial T}{\partial y}=\alpha(\frac{\partial^2 T}{\partial x^2}+\frac{\partial^2 T}{\partial y^2})\,.$$

Radiation heat transfer by the glass cover surface must account for thermal radiation which can be absorbed, reflected, or transmitted. This decomposition can be expressed by:

$$q_{net}=q_{absorbed}+q_{transmitted}+q_{reflected}\,.$$

The amount of reflected energy from glass surface to outside the boundary layer $q_{reflected}$ is:

$$q_{reflected}=q_r=-hA(T_w-T_a)\,.$$

Now the amount of transmitted energy reaches from the cover plate to the absorber without any medium as:

$$q_{transmitted}=q_t=\epsilon\sigma I A\,.$$

Here ϵ is emissivity of the glass cover plate, σ is the absorption rate of the absorber, I is the solar irradiation and and T_w is the variable temperature of the glass cover plate. Again, the amount of absorbed energy is transferred from cover plate to absorber by natural convection as:

$$q_{absorbed}=q_a=hA(T_w-T_i)\,.$$

So total energy gained or lost by the cover plate is:

$$q_{net}=hA(T_w-T_i)+\epsilon\sigma I A-hA(T_w-T_a)\,.$$

The boundary conditions are:

- at all solid boundaries: $u=v=0\,,$
- at the vertical walls $\frac{\partial T}{\partial X}=0\,,$
- at the top cover plate:

$$q=hA(T_w-T_i)+\epsilon\sigma I A-hA(T_w-T_a)\,,$$

- at the bottom wavy absorber: $T=T_c\,.$

The above equations are non-dimensionally by using the following dimensionless dependent and independent variables:

$$X=\frac{x}{L},Y=\frac{y}{L},U=\frac{uL}{\nu},V=\frac{vL}{\nu}\,,$$

$$P=\frac{pL^2}{\rho\nu^2},\theta=\frac{(T-T_c)k}{qL}\,.$$

Then the dimensionless governing equations are:

$$\frac{\partial U}{\partial X}+\frac{\partial V}{\partial Y}=0\,, \tag{3.1}$$

$$U\frac{\partial U}{\partial X}+V\frac{\partial U}{\partial Y}=-\frac{1}{\rho}\frac{\partial P}{\partial X}+\nu(\frac{\partial^2 U}{\partial X^2}+\frac{\partial^2 U}{\partial Y^2}) \tag{3.2}$$

$$U\frac{\partial V}{\partial X}+V\frac{\partial V}{\partial Y}=-\frac{1}{\rho}\frac{\partial P}{\partial Y}+\nu(\frac{\partial^2 V}{\partial X^2}+\frac{\partial^2 V}{\partial Y^2})+\frac{Ra}{Pr}\theta \tag{3.3}$$

$$U\frac{\partial \theta}{\partial X}+V\frac{\partial \theta}{\partial Y}=\frac{1}{Pr}(\frac{\partial^2 \theta}{\partial X^2}+\frac{\partial^2 \theta}{\partial Y^2}) \tag{3.4}$$

where $Pr=\frac{\nu}{\alpha}$ is the Prandtl number, $Ra=\frac{g\beta L^4 q}{\nu\alpha k}$ is the Rayleigh number.

The consequent boundary conditions get the form:

- at all solid boundaries: $U=V=0\,,$
- at the absorber surface: $\theta=0\,,$
- at the top glass surface: $\frac{\partial\theta}{\partial Y}=-1\,,$
- at the vertical surfaces: $\frac{\partial\theta}{\partial X}=0\,.$

The shape of the bottom wavy absorber profile is assumed to mimic the pattern $Y=A_m[1-\cos(2\lambda\pi X)]$ where A_m is the dimensionless amplitude of the wavy surface and λ is the number of undulations. $Ar(=L/H)$ is the aspect ratio of the air layer. Aspect ratio $Ar=11$, amplitude of wave $A_m=0.04$ and number of wave $\lambda=3.5$ are assumed. L and H are length and average height of this physical model, respectively.

3.1. **Average Nusselt number.** The average Nusselt number (Nu) is expected to depend on a number of factors such as thermal conductivity, heat capacitance, viscosity, flow structure of fluid. The non-dimensional form of local convective heat transfer taken at the upper surface can be written as $\overline{Nu_c} = -\frac{\partial\theta}{\partial Y}$. By integrating the local convective Nusselt number over the top heated surface, the average convective heat transfer along the top wall of the solar collector is $Nu_c = \int_0^1 \overline{Nu_c}\, dX$. The radiative heat transfer rate at the top cover plate is expressed as $Nu_r = \int_0^1 q_r dX$. The average Nusselt number at the top surface is assumed as $Nu = Nu_c$.The mean bulk temperature and average sub-domain velocity of the fluid inside the collector may be written as $\theta_{av} = \int \theta d\overline{V}/\overline{V}$ and $V_{av} = \int \mathrm{V} d\overline{V}/\overline{V}$, where $\overline{V}$ is the volume of the solar collector.

4. NUMERICAL IMPLEMENTATION

The Galerkin finite element method of Taylor and Hood [22] and Dechaumphai [23] is used to solve the non-dimensional governing equations along with boundary conditions for the considered problem. The equation of continuity has been used as a constraint due to mass conservation and this restriction may be used to find the pressure distribution. This method is used to solve the equation (3.1)-(3.4), where the pressure P is eliminated by a constraint ξ and the incompressibility criteria given by equation (3.1) can be expressed as:

$$P = -\xi(\frac{\partial U}{\partial X} + \frac{\partial V}{\partial Y}).$$

The continuity equation is automatically fulfilled for large values of ξ. Then the velocity components (U, V) and temperature (θ) are expanded using a basis set $\{\Phi\}_{k=1}^{N}$ as:

$$\begin{aligned} U &\approx \sum_{k=1}^{N} U_k \Phi_k(X,Y) \\ V &\approx \sum_{k=1}^{N} V_k \Phi_k(X,Y) \\ \theta &\approx \sum_{k=1}^{N} \theta_k \Phi_k(X,Y). \end{aligned} \tag{4.1}$$

The Galerkin finite element technique yields the subsequent nonlinear residual equations for the equations (3.2), (3.3) and (3.4) respectively at nodes of the internal domain Ω:

$$\begin{aligned} R_i^{(1)} &= \sum_{k=1}^{N} U_k \int_\Omega \left[\left(\sum_{k=1}^{N} U_k \Phi_k \right) \frac{\partial \Phi_k}{\partial X} + \right. \\ &\quad \left. + \left(\sum_{k=1}^{N} V_k \Phi_k \right) \frac{\partial \Phi_k}{\partial Y} \right] \Phi_i dX dY \\ &\quad -\xi \frac{1}{\rho} \left[\sum_{k=1}^{N} U_k \int_\Omega \frac{\partial \Phi_i}{\partial X} \frac{\partial \Phi_k}{\partial X} dX dY + \right. \\ &\quad \left. + \sum_{k=1}^{N} V_k \int_\Omega \frac{\partial \Phi_i}{\partial Y} \frac{\partial \Phi_k}{\partial Y} dX dY \right] \\ &\quad -\nu \sum_{k=1}^{N} U_k \int_\Omega [\frac{\partial \Phi_i}{\partial X} \frac{\partial \Phi_k}{\partial X} + \frac{\partial \Phi_i}{\partial Y} \frac{\partial \Phi_k}{\partial Y}] dX dY ; \end{aligned} \tag{4.2}$$

$$\begin{aligned} R_i^{(2)} &= \sum_{k=1}^{N} V_k \int_\Omega \left[\left(\sum_{k=1}^{N} U_k \Phi_k \right) \frac{\partial \Phi_k}{\partial X} + \right. \\ &\quad \left. + \left(\sum_{k=1}^{N} V_k \Phi_k \right) \frac{\partial \Phi_k}{\partial Y} \right] \Phi_i dX dY - \\ &\quad -\xi \frac{1}{\rho} \left[\sum_{k=1}^{N} U_k \int_\Omega \frac{\partial \Phi_i}{\partial X} \frac{\partial \Phi_k}{\partial X} dX dY + \right. \\ &\quad \left. + \sum_{k=1}^{N} V_k \int_\Omega \frac{\partial \Phi_i}{\partial Y} \frac{\partial \Phi_k}{\partial Y} dX dY \right] - \\ &\quad -\nu \sum_{k=1}^{N} V_k \int_\Omega \left[\frac{\partial \Phi_i}{\partial X} \frac{\partial \Phi_k}{\partial X} + \frac{\partial \Phi_i}{\partial Y} \frac{\partial \Phi_k}{\partial Y} \right] dX dY + \\ &\quad + \frac{Ra}{Pr} \int_\Omega (\sum_{k=1}^{N} \theta_k \Phi_k) \Phi_i dX dY ; \end{aligned} \tag{4.3}$$

$$\begin{aligned} R_i^{(3)} &= \sum_{k=1}^{N} \theta_k \int_\Omega \left[\left(\sum_{k=1}^{N} U_k \Phi_k \right) \frac{\partial \Phi_k}{\partial X} + \right. \\ &\quad \left. + \left(\sum_{k=1}^{N} V_k \Phi_k \right) \frac{\partial \Phi_k}{\partial Y} \right] \Phi_i dX dY - \\ &\quad - \frac{1}{Pr} \sum_{k=1}^{N} \theta_k \int_\Omega \left[\frac{\partial \Phi_i}{\partial X} \frac{\partial \Phi_k}{\partial X} + \frac{\partial \Phi_i}{\partial Y} \frac{\partial \Phi_k}{\partial Y} \right] dX dY . \end{aligned} \tag{4.4}$$

Three points Gaussian quadrature is used to evaluate the integrals in these equations. The non-linear residual equations (4.2), (4.3) and (4.4) are solved using Newton-Raphson method to determine the coefficients of the expansions in equation (4.1). The convergence of solutions is assumed when the relative error for each variable between consecutive iterations is recorded below the convergence criterion ϵ such that $\mid \Psi^{n+1} - \Psi^n \mid \leq 10^{-4}$, where n is the number of iteration and Ψ is a function of U, V and θ.

4.1. **Mesh Generation.** In the finite element method, the mesh generation is the technique to subdivide a domain into a set of sub-domains, called finite elements, control volume, etc. The discrete locations are defined by the numerical grid, at which the variables are to be calculated. It is basically a discrete representation of the geometric domain on which the problem is to be solved. The computational domains with irregular geometries by a collection of finite elements make the method a valuable practical tool for the solution of boundary value problems arising in various fields of engineering. Fig. 2 displays the finite element mesh of the present physical domain. Here the computational domain is discretized into unstructured triangles.

Fig. 2: Mesh generation of the air

4.2. **Grid Independent Test.** An extensive mesh testing procedure is conducted to guarantee a grid-independent solution for $Pr = 0.7$ and $Ra = 10^5$ in a thin air space. In the present study, we examine five different non-uniform grid systems with the following number of elements within the resolution field: $2880, 4830, 6516, 8157$ and 10482. The numerical scheme is carried out for highly precise key in the average convective and radiative Nusselt numbers, namely, Nu_c and Nu_r for the aforesaid elements to develop an understanding of the grid fineness as shown in Table 1. The scale of the average Nusselt number (convective and radiative) for 8157 elements shows a little difference with the results obtained for the other elements. Hence, considering the non-uniform grid system of 8157 elements is preferred for the computation.

Table 1: Grid Sensitivity Check at $Pr = 0.7$ and $Ra = 10^5$.

Elements	Nu_c	Nu_r	Time (s)
2880	4.32945	2.32945	248.265
4830	5.0176	2.78176	301.594
6516	5.77701	3.38701	395.157
8157	6.35549	3.82491	482.328
10482	6.35555	3.82498	618.375

4.3. **Code Validation.** The present numerical solution is validated by comparing the current code results for heat transfer - temperature difference profile at $Pr = 0.73$, $Gr = 10^4$ with the graphical representation of Gao et al. [24] which was reported for heat transfer augmentation inside a channel between the flat-plate cover and sine-wave absorber of a cross-corrugated solar air heater.

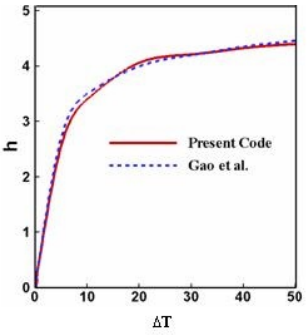

Fig. 3: Comparison between present code and Gao et al. [24] at $Pr = 0.73$ and $Ra = 10^4$

Fig. 3 demonstrates the above stated comparison. As shown in Fig. 4, the numerical solutions (present work) and Gao et al. [24]are in good agreement. In addition, the current code results for streamlines and isotherms at $Pr = 0.71$, $A = 2$, $L = 2$, $\phi = 40^0$, $Ra = 10^6$ with that of Varol and Oztop [18] are compared and displayed by Fig. 4. They studied Buoyancy induced heat transfer and fluid flow inside a tilted wavy solar collector.

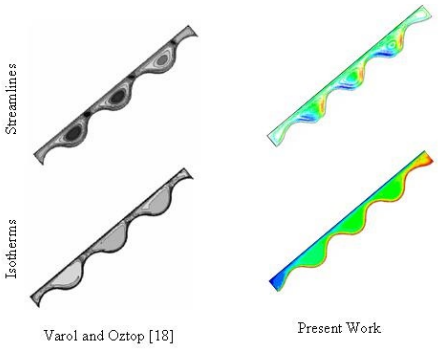

Fig. 4: Comparison of present code with Varol and Oztop [18]

5. RESULTS AND DISCUSSION

In this section, numerical results of temperature and velocity profiles in terms of isotherms and streamlines for various values of convective parameter Ra across air space of the solar collector are displayed. The considered values of Ra are $Ra = 10^4, 10^5, 10^6, 5 \times 10^6$ while the Prandtl number $Pr = 0.7$, solar irradiation $I = 600 Wm^{-2}$, absorption rate

of absorber $\sigma = 0.95$ and the emissivity $\epsilon = 0.95$ are kept fixed.

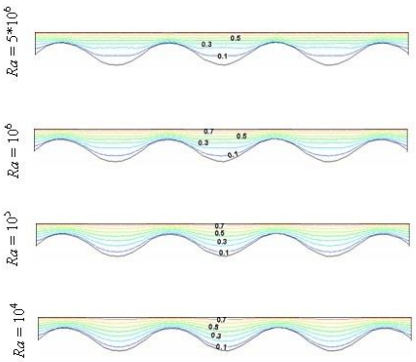

Fig. 5: Effect of Ra on isothermal lines of air

In addition, the values of the average Nusselt number both for convection and radiation, mean bulk temperature and average velocity of air as well as mid height horizontal and vertical velocities are shown graphically for the pertinent parameter Ra.

The effect of Ra on the thermal lines is presented in Fig. 5 while $Pr = 0.7$, $\epsilon = 0.98$, $A_m = 0.04$, $\lambda = 3.5$, $Ar = 11$. The values of Rayleigh number are considered as $10^4, 10^5, 10^6, 5 \times 10^6$. In the Fig. 5 the label in the isothermal lines indicates the number of lines in order. Initially isothermal lines appear the whole domain of the collector. Due to the effect of buoyancy in free convection heat transfer, they tend to gather the heated top surface. Also a thin thermal boundary layer is developed near the upper pick of each wave. This happens because of escalating Rayleigh number enhances the buoyancy force of the working fluid air. Then this force hits the fluids in upward direction. This procedure continues till the temperature gradient occurs.

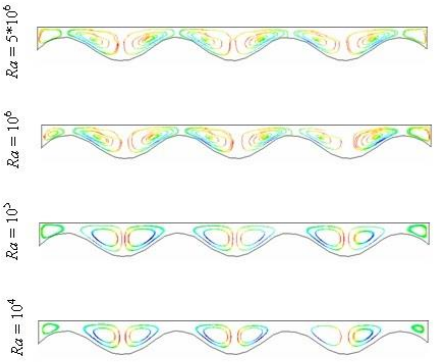

Fig. 6: Effect of Ra on streamlines of air

On the other hand, the streamlines are expressed in Fig. 6 for the variation of buoyancy convective parameter Ra. Six primary recirculation cells occupying the whole domain are found at the lowest value of the Rayleigh number ($Ra = 10^4$) in Fig. 6. In each wave, the right and left vortices rotate in the counter-clockwise and clockwise direction, respectively. Due to significant effect of free convection two secondary circulatory flows are developed at the left and right top corner of the domain in this case. The size of these cells becomes larger with the variation of free convection. For increasing value of Ra, velocity of air also increases and thus size of the created eddies becomes larger. In addition, more perturbation is observed in the streamlines at $Ra = 5 \times 10^6$ because of rising buoyancy force.

The average Nusselt number for convection and radiation, average temperature (θ_{av}) and mean sub-domain velocity (V_{av}) profile along with the Rayleigh number (Ra) for air ($Pr = 0.7$) are depicted in Fig. 7(i)-(iii). In Fig. 7(i), it is seen that Nu_c and Nu_r enhance gradually due to effective buoyancy force.

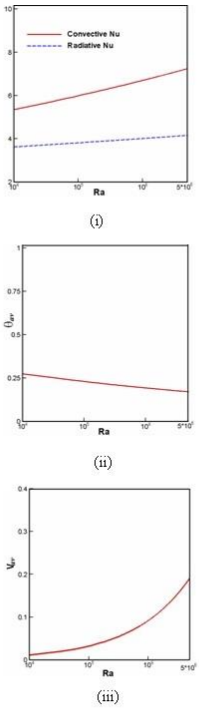

Fig. 7: Effect of Ra on (i) average Nusselt number, (ii) mean temperature and (iii) mean velocity of air

The increasing rate of heat transfer for air is found to be effective. Rate of convective heat transfer enhances by 26 percent whereas this rate for radiation is 14 percent with the variation of Ra from 10^4 to 5×10^6. It is well known that heat transfer rate is always higher for convection than radiation and is justified by the current investigation. Consequently Fig. 7(ii) shows that (θ_{av}) falls sequentially for all Ra. Fig. 7(iii) describes the enhancing phenomena

in the V_{av}-Ra profile. It is observed that the magnitude of mean velocity graph is in parabolic shape.

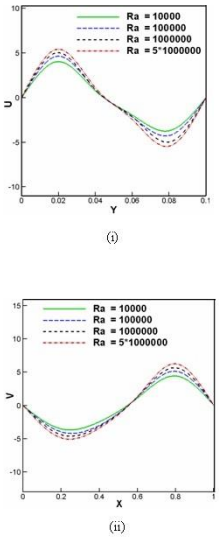

Fig. 8: Effect of Ra on mid height (i) U velocity and (ii) V velocity

The mid height horizontal (U) velocity at $X = 0.5$ and vertical (V) velocity at $Y = 0.05$ of the solar collector for various Ra is displayed in Fig. 8 (i)-(ii). Significant variation in velocity is found due to changing Ra. In the case of Fig. 8(i) for the effect of Ra some perturbations are seen in the U-Y graph. The waviness in the V-X profile devalues for lower values of Ra.

6. Correlation

On the basis of the current numerical study the calculated average Nusselt number Nu is correlated with Rayleigh number Ra and Prandtl number Pr. Here the parametric values are taken as $0.071 \leq Pr \leq 0.73$, $10^3 \leq Ra \leq 10^5$, $Ar = 17$, $A_m = 0$, $\lambda = 0$ and $\epsilon = 0$. This correlation can be written as follows:

$$Nu = [0.6542 + 0.3061Pr](Ra)^{0.1730} \tag{6.1}$$

where the confidence coefficient for the above equation is $R^2 = 98.30$ percent.

7. Semi-empirical Relation

A new experimental measurement on free convection heat transfer rates through inclined air layers of high aspect ratio and heated from below is represented by Hollands et al. [21]. They established a relation between Nu and Ra for tilt angles ranging from 0^0 to 75^0 as:

$$\begin{aligned} Nu &= 1 + 1.14\left(1 - \frac{1708(\sin 1.8\phi)^{1.6}}{(Ra)\cos\phi}\right) \times \\ &\times \left[1 - \frac{1708}{(Ra)\cos\phi}\right]^{+} + \left[\left(\frac{(Ra)\cos\phi}{5830}\right)^{1/3} - 1\right], \end{aligned}$$

where the $+$ exponent indicates that only positive values for terms within square brackets are to be used; in case of negative values, zero is used.

The above equation was used frequently for the purpose of experimental studies of solar collector by various authors such as Lior [25], Azad [26], Gang et al. ([27],[28]), Saleh [29], etc.

For horizontal solar collector $\phi = 0^0$, the above equation becomes:

$$\begin{aligned} Nu &= 1 + 1.14\left[1 - \frac{1708}{Ra}\right]^{+} + \\ &+ \left[\left(\frac{Ra}{5830}\right)^{1/3} - 1\right]. \end{aligned} \tag{7.1}$$

The above equation is significant for air through solar collector of high aspect ratio in the range of natural convective parameter $10^3 \leq Ra \leq 10^5$.

A semi-empirical relation is established from the correlation of the equation (6.1) with the experimental data provided by the equation (7.1) of Hollands et al. [21] which can be written as:

$$Nu = -1.1167 + [0.4936 + 0.23095Pr]\,(Ra)^{0.1730}. \tag{7.2}$$

8. Comparison with Experimental Result

The present results are compared with the experimental results available in the literature.

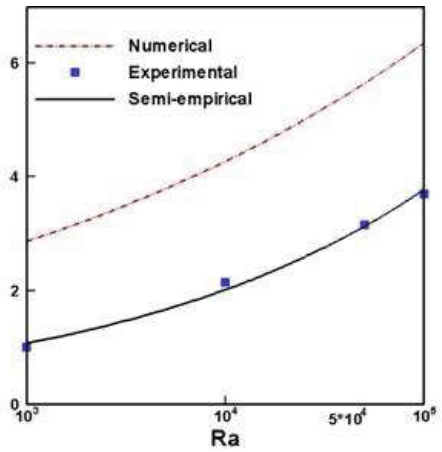

Fig. 9: Nu at different Ra from the equation (7.1) of Hollands et al. and equations (6.1) and (7.2) of present study

Table 2 provides the values of average Nusselt number from the experimental result as per equation (7.1) of Hollands et al. [21], the numerical results from equation (6.1) and the semi-empirical result as in equation (7.2). Value of $Pr = 0.7$ is used in equation (6.1) and equation (7.2).

In Fig. 9 the graphical representation of the average Nusselt number (Nu) corresponding to Table 2 has been shown. This Fig. 9 demonstrates a good agreement between the experimental result and that obtained by the semi-empirical relation from the current study.

Table 2: Values of Nu at different Ra from equation (7.1) of Hollands et al. [21] and equations (6.1) and (7.2) of present study.

Ra	Eq. (7.1)	Eq. (6.1)	Eq. (7.2)
10^3	1	2.8285	1.0481
10^4	2.1442	4.4743	2.1074
5×10^4	3.1480	5.3221	3.1426
10^5	3.6995	6.5371	3.6852

Conclusion

The free convective flow and heat transfer for the effect of Rayleigh number across a thin air space of the solar collector are accounted. Various Ra have been considered for the flow and temperature fields as well as the convective heat transfer rates, mid height horizontal and vertical velocities, mean bulk temperature of fluid and average velocity field inside the wavy solar collector. The numerical results lead to the following conclusions:

- The free convection parameter Ra has a significant effect on the flow and temperature fields. Size of buoyancy-induced vortex in the streamlines is increased and thermal layer near the heated surface becomes thick with increasing Ra.
- The highest heat transfer rate is observed for the greatest Ra.
- Increasing values of Ra devalues mean bulk temperature of air.
- Mean velocity rises with increasing values of Ra.
- More considerable changes occur in the mid-height horizontal and vertical velocity profiles of air at $Ra = 5 \times 10^6$.

Acknowledgment

This work is done in the Department of Mathematics, Bangladesh University of Engineering and Technology, Dhaka-1000, Bangladesh. This research article is supported by the Research Support and Publication Division, University Grants Commission, Agargaon, Dhaka, Bangladesh.

References

[1] SP. Sukhatme: *Solar energy, principles of thermal collection and storage*, Tata McGraw-Hill, New Delhi, 1991.

[2] J.A. Stasiek: *Experimental studies of heat transfer and fluid flow across corrugated-undulated heat exchanger surfaces*, Int. J. of Heat and Mass Trans., **41** (1998), 899–914.

[3] S. Noorshahi, C.A. Hall, E.K. Glakpe: *Natural Convection in a Corrugated Enclosure with Mixed Boundary Conditions*, ASME J. of Solar Energy Engg., **118** (1996), 50–57.

[4] W. Gao: *Analysis and performance of a solar air heater with cross corrugated absorber and back-plate*, MS thesis, Yunnan Normal University, Kunming, 1996.

[5] W. Xiaowu, B. Hua: *Energy analysis of domestic-scale solar water heaters*, Renew. Sust. Energy Rev., **9** (6) (2005), 638–645.

[6] W. Xuesheng, W. Ruzhu, W. Jingyi: *Experimental investigation of a new-style double-tube heat exchanger for heating crude oil using solar hot water*, Appl. Therm. Eng., **25** (11-12) (2005), 1753–1763.

[7] C.D. Ho, T.C. Chen: *The recycle effect on the collector efficiency improvement of double-pass sheet-and-tube solar water heaters with external recycle*, Renew. Energy, **31**(7) (2006), 953–967.

[8] A. Hussain: *The performance of a cylindrical solar water heater*, Renew. Energy, **31** (11) (2006), 1751–1763.

[9] G. Hetsroni, R. Rozenblit: *Heat transfer to a liquid-solid mixture in a flume*, Int. J. Multiph. Flow, **20**(4) (1994), 671–689.

[10] Y. Tripanagnostopoulos, M. Souliotis, T. Nousia: *Solar collectors with colored absorbers*, Solar Energy, **68** (2000), 343–356.

[11] Z.C. Orel,M.K. Gunde, M.G. Hutchins:: *Spectrally selective solar absorbers in different non-black colours*, Proc. of WREC VII, Cologne on CD-ROM, 2002.

[12] J. Wazwaz, H. Salmi, R. Hallak: *Solar thermal performance of a nickel-pigmented aluminium oxide selective absorber*, Renew. Energy, **27** (2002), 277–292.

[13] P. Konttinen, P.D. Lund, R.J. Kilpi: *Mechanically manufactured selective solar absorber surfaces*, Solar Energy Mater Solar Cells, **79** (3) (2003), 273–283.

[14] H. Soltau: *Testing the thermal performance of uncovered solar collectors*, Solar Energy, **49** (4) (1992), 263–272.

[15] B. Molineaux, B. Lachal, O. Gusian: *Thermal analysis of five outdoor swimming pools heated by unglazed solar collectors*, Solar Energy, **53** (1)(1994), 21–26.

[16] A. Kolb, E.R.F. Winter, R. Viskanta: *Experimental studies on a solar air collector with metal matrix absorber*, Solar Energy, **65** (2) (1999), 91–98.

[17] E.F. Kent: *Numerical analysis of laminar natural convection in isosceles triangular enclosures for cold base and hot inclined walls*, Mech. Res. Commun., **36** (2009), 497–508.

[18] Y. Varol, H.F. Oztop: *Buoyancy induced heat transfer and fluid flow inside a tilled wavy solar collector*, Build. Environ., **42** (2007), 2062–2071.

[19] O.A. Beg, A. Bakier, R. Prasad, S.K. Ghosh: *Numerical modelling of non-similar mixed convection heat and species transfer along an inclined solar energy*

collector surface with cross diffusion effects, World J. of Mech., **1**, (2011), 185–196.

[20] R. Nasrin: *Influences of physical parameters on mixed convection in a horizontal lid driven cavity with undulating base surface*, Num. Heat Trans., **61** (2012), 306–321.

[21] K.G.T. Hollands, T.E. Unny, G.D. Raithby, L. Konicek: *Free convection heat transfer across inclined air layers*, Trans. of the American Soc. of Mech. Engineers, J. of Heat Trans., **98** (1976), 189–193.

[22] C. Taylor, P. Hood: *A numerical solution of the Navier-Stokes equations using finite element technique*, Computer and Fluids, **1** (1973), 73–89.

[23] P. Dechaumphai: *Finite Element Method in Engineering, 2nd ed.*, Chulalongkorn University Press, Bangkok, 1999.

[24] W. Gao, W. Lin, E. Lu: *Numerical study on natural convection inside the channel between the flat-plate cover and sine-wave absorber of a cross-corrugated solar air heater*, Energy Conversion and Management, **41** (2000), 145–151.

[25] N. Lior: *Thermal theory and modeling of solar collectors*, Energy Storage and Materials, MIT Press, Cambridge MA, 100-182.

[26] E. Azad: *Interconnected heat pipe solar collector*, IJE Transactions A: Basics, **22**(3) (2009), 233–242.

[27] P. Gang, F. Huide, Z. Huijuan, J. Jie: *Performance study and parametric analysis of a novel heat pipe PV/T system,*, J. of Energy, doi:10.1016/j.energy.2011.11.017 (2011), 1–12.

[28] P. Gang, F. Huide, Z. Tao, J. Jie: *A numerical and experimental study on a heat pipe PV/T system,*, Solar Energy, **85** (2011), 911–921.

[29] A.M. Saleh: *Modeling of flat-plate solar collector operation in transient states*, M. Sc. in Engg. Thesis, Purdue University, Fort Wayne, Indiana.

Department of Mathematics
Bangladesh University of Engineering and Technology
Dhaka-1000, Bangladesh
E-mail address: raity11@gmail.com

Department of Mathematics
Bangladesh University of Engineering and Technology
Dhaka-1000, Bangladesh
E-mail address: fariduddin1972@gmail.com

Department of Mathematics
Bangladesh University of Engineering and Technology
Dhaka-1000, Bangladesh
E-mail address: a0alim@gmail.com